

Twinning in vapour-grown, large volume Cd_{1-x}Zn_xTe crystals

B K Tanner^{1*}, J T Mullins², A T G Pym² and D Maneuski³

¹*Department of Physics Durham University, South Road, Durham, DH1 3LE, U.K.*

²*Kromek Group plc, Thomas Wright Way, NETPark, Sedgefield, County Durham, TS21 3FD, U.K.*

³*SUPA, Department of Physics and Astronomy, University of Glasgow, Glasgow G12 8QQ, U.K.*

Abstract

The onset of twinning from $(\bar{2}\bar{1}\bar{1})$ to $(\bar{1}\bar{3}\bar{3})$ in large volume Cd_{1-x}Zn_xTe crystals, grown by vapour transport on $(\bar{2}\bar{1}\bar{1})$, often referred to as (211)B, oriented GaAs seeds, has been investigated using X-ray diffraction imaging (X-ray topography). Twinning is not associated with strains at the GaAs/CdTe interface as the initial growth was always in $(\bar{2}\bar{1}\bar{1})$ orientation. Nor is twinning related to lattice strains associated with injection of Zn subsequent to initial nucleation and growth of pure CdTe as in both cases twinning occurred after growth of several mm length of Cd_{1-x}Zn_xTe. While in both cases examined, there was a region of disturbed growth prior to the twinning transition, in neither crystal does this strain appear to have nucleated the twinning process. In both cases, un-twinned material remained after twinning was observed, the scale of the resulting twin boundaries being sub-micron. Simultaneous twinning across the whole sample surface was observed in one sample, whereas in the other, twinning was nucleated at different points and times in the growth.

*Corresponding author: b.k.tanner@dur.ac.uk

Keywords: A1.X-ray topography, A2.Growth from vapour, B1.Tellurides, B2.Semiconducting II-VI materials

1. Introduction

The semiconductor Cd_{1-x}Zn_xTe (CZT) is becoming an increasingly important material for energy sensitive X and γ -ray detection, for example in medical and nuclear contexts. However, its commercial adoption has been slow, primarily on grounds of cost but also because of deficiencies in material properties. For commercial viability, both the perfection and the size of crystals must be improved.

Spectrometer-grade CZT can be produced by the high pressure Bridgman technique [1,2,3] but growth of crystals with low dislocation density and free from Te precipitates [4] and inclusions has been challenging [5,6,7,8], particularly as the boule diameter has been scaled up. 100 mm diameter bulk crystals of Cd_{1-x}Zn_xTe have been grown successfully by two techniques, the travelling heater method (THM) [9,10] and the multi-tube physical vapour transport technique (MTPVT) [11]. These techniques have changed the economic viability of the application of Cd_{1-x}Zn_xTe. Recently,

Schneider *et al.* [12] reported a comparison of the excited state recombination lifetimes of the two types of material using fluorescence lifetime imaging microscopy. In both cases, two decay lifetimes, one short and one long, were identified. Although, for the majority of the MTPVT-grown $\text{Cd}_{1-x}\text{Zn}_x\text{Te}$, their values were similar to those in THM grown material, in the early stage growth of MTPVT growth, both lifetimes were significantly extended. This may be associated with defects generated in twinned regions or interfaces in $(\bar{2}\bar{1}\bar{1})$, also known as (211B), oriented MTPVT material, as growth proceeds and this paper reports an investigation into the distribution of twins following this transition. We have previously shown that for MTPVT-grown ZnTe, where $x=1$, no such twinning transition could be observed [13]. It appeared that either the ZnTe crystal nucleated on the GaAs substrate in the $(\bar{1}\bar{3}\bar{3})$ orientation, or that the flip to this orientation occurred within a very short, micrometre-scale, distance of the seed.

Vapour growth does not suffer from incorporation of Te inclusions and use of a heterogeneous seed permits growth of large diameter crystals. However, past attempts at vapour growth have been frustrated by the inability to control independently the source and seed temperatures, and the transport rate. We have successfully grown CdTe [14] and CZT crystals [15,11] up to 100mm diameter on GaAs substrates, using a multi-tube physical vapour transport (MTPVT) technique [16,17]. The key feature of the growth system is that the temperatures of source and seed are thermally decoupled by use of independent vertical furnaces which are parallel, separated horizontally and interconnected by a horizontal, heated, transport tube to avoid any line of sight, and thus radiative thermal coupling, between source and seed. The growth envelope is constructed from quartz and together with the surrounding heating elements is contained within an evacuated and cooled stainless steel chamber. Flow restrictors incorporated into the horizontal transport tube effectively de-couple the mass transport from the source-sink temperature difference making the growth process highly controllable.

Both $\text{Cd}_{1-x}\text{Zn}_x\text{Te}$ and CdTe crystals grown by MTPVT on (211)B GaAs substrates exhibit a tendency to twin to the $[\bar{1}\bar{3}\bar{3}]$ orientation with respect to the growth direction. The twin boundaries lie on two common {111} planes intersecting the growing surface. In the case of the binary CdTe, such twinning may be observed at any stage from nucleation to the bulk growth phase. Despite this, untwinned CdTe boules up to 8 mm thick have been grown and have been shown to have high structural perfection [14]. In contrast, $\text{Cd}_{1-x}\text{Zn}_x\text{Te}$ grown on (211)B CdTe buffer layers invariably twins mainly but not entirely to $(\bar{1}\bar{3}\bar{3})$. This twinning is accompanied by triangular or pyramidal facet development in the $[\bar{1}\bar{1}\bar{1}]$ direction, which smooths out as growth proceeds. Infra-red mapping of the regions in which twinning is observed reveals opaque features which replicate the geometry of the facets and imply a discontinuity in the lattice. These features appear to comprise voids or polycrystalline regions. The structural perfection of $\text{Cd}_{1-x}\text{Zn}_x\text{Te}$ growing in this orientation generally reduces as the crystal grows.

The orientation flip does not occur during nucleation but when a substantial length of crystal has been grown. The onset of twinning can be detected by high resolution X-ray diffraction (HRXRD) but the relatively large beam size means that the scale of the twinning cannot be determined at sub-millimetre level. It is also difficult to

understand from the HRXRD scans how other defects, such as low angle boundaries, relate to the twinning behaviour. As part of our programme of continuous improvement of the MTPVT process, where structural information is fed back into the crystal growth, we have performed X-ray diffraction imaging (topography) at beamline B16 of the Diamond Light Source. We have studied the development of the twins and the relative distribution of untwinned oriented material following the switch to the twinned orientation, plus the effect of abrupt Zn injection, if any, on the twinning.

2. X-ray Diffraction Imaging

X-ray diffraction imaging, otherwise known as X-ray diffraction topography, has been used for very many years to observe crystal lattice defects through the scattering of X-rays from their surrounding strain fields [18]. However, the extremely angular high sensitivity of X-ray diffraction to strain is deleterious to high spatial resolution of individual defects, with a consequence that individual dislocations cannot be imaged in relatively imperfect materials such as CZT, although macroscopic twin boundaries and low angle boundaries can be revealed in this material [19]. A major problem with the white radiation imaging method, commonly used at synchrotron radiation sources for its simplicity and flexibility, is that the local strains in the material can be extremely high, resulting in substantial asterism. Thus it has been extremely difficult to interpret the images, as exemplified by the synchrotron radiation studies of Egan *et al.* [20] and Palosz *et al.* [21] on CZT crystals grown by vapour transport. The asterism arises because X-rays diffracted from the distorted regions of the crystal have significantly different energy to those diffracted by unstrained material. As the Bragg angle therefore differs, the diffracted intensity is displaced with respect to its location on the main image, leading to asterism streaks which, when they overlap, can give the impression of localized defects.

A solution to the problem of asterism is to use radiation monochromated by diffraction from a pair of 111 Si crystals, a standard configuration on many synchrotron radiation beamlines. However, in this configuration, for crystals as defective as CZT, only a small region will satisfy the Bragg condition (Fig. 1), resulting in a stripe of intensity across the image. This represents a contour of equal effective misorientation. The effective misorientation $\Delta\theta$ represents a combination of tilt $\delta\theta$ and dilation δd of Bragg planes of spacing d such that,

$$\Delta\theta = \frac{\delta d}{d} \tan \theta_B \pm \delta\theta \quad \text{Eq. 1}$$

where θ_B is the Bragg angle. In the case of the MTPVT-grown CZT crystal shown, the stripe is not straight, indicating that quite complex distortions are present. While contrast can be seen across the stripe, it is not easily interpreted with respect to the crystal as a whole as most of the crystal surface does not diffract strongly. We also note that the width of the intensity stripe varies quite dramatically across the crystal, showing that the distortion to the left of the image is less than that on the right side. (The narrower the width of the intensity stripe, the more distorted is the crystal.)

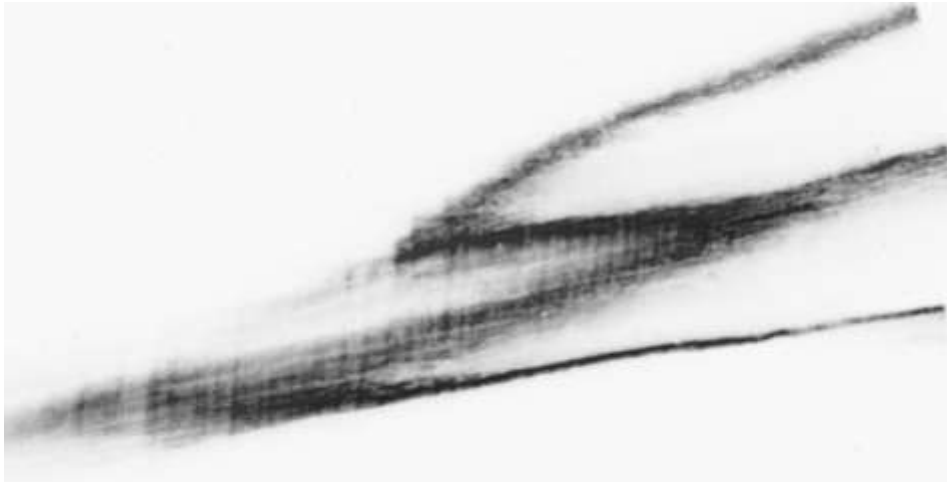


Fig.1 X-ray diffraction image, taken in back reflection with a wide area monochromatic beam, of a CZT crystal grown by MTPVT. 400 reflection from $(\bar{1}11)$ face of CZT, 10keV X-ray energy. The frame is 9 mm in width and due to geometrical compression, the image represents 9 mm in height. Note that, as in all images, the projection of the diffraction vector is vertically upwards.

In the 1960s Renninger used this contour of equal misorientation to map the long range distortion across crystals by the simple expedient of displacing the crystal with respect to the incident beam and recording multiple images on a single photographic emulsion [22,23]. The larger the angular step, the greater was the displacement of the effective misorientation contours. These he called “Zebra Patterns” as the result is reminiscent of the stripes on the zebra animal. The method was subsequently used by others, for example, on Si [24,25,26] and GaAs [27]. With modern electronic imaging detectors, it is easy to record the contour of equal misorientation and follow its translation across the crystal as the incidence angle is stepped with respect to the incident beam, i.e. across the rocking curve [28]. Addition of selected images immediately produces a “Zebra Pattern” mapping the effective misorientation across the whole crystal surface (Fig. 2). The technique has been used successfully with vapour-grown ZnTe [13] and as a means of building up an image across a highly deformed surface of crystals of $\text{Cd}_{1-x}\text{Zn}_x\text{Te}$ grown by the travelling heater method [29].

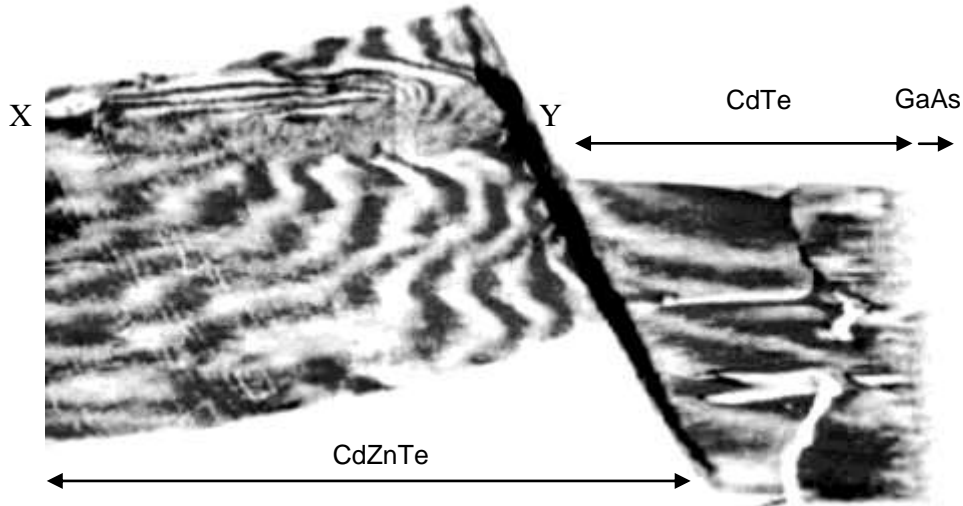


Fig. 2 Renninger “Zebra Pattern” [3] of contours of effective misorientation from superposition of every 8th frame, in 7.2 arc second steps, across the rocking curve. $0\bar{2}2$ reflection from $(0\bar{1}1)$ C face of CZT sample number 69-1, 10keV X-ray energy. The image shows both $(\bar{2}\bar{1}\bar{1})$ and $(\bar{1}\bar{3}\bar{3})$ material. Image displacement occurs because of the change of lattice constant due to the intentionally abrupt Zn injection. The image represents 9 mm in width and 11 mm in height.

3. Experimental Methods

We have used such high resolution monochromatic beam X-ray diffraction imaging to study the development of the twins and the effect of rapid injection of Zn into what were initially CdTe crystals grown on $(\bar{2}\bar{1}\bar{1})$ oriented substrates by MTPVT. All images were taken in the Bragg (reflection) geometry using the Huber diffractometer at beamline B16 of the Diamond Light Source at Didcot, U.K. The incident beam was monochromated by a pair of independently tuned 111 Si reflections, oriented to select an energy of 10keV, i.e. a wavelength of 0.124nm. The imaging detector was a Photonic Science SCMOS camera with a pixel pitch of 3.25 μ m. All topographs in this paper are shown as positives (with enhanced intensity darker) and as if looking towards the X-ray source. The incidence plane, and hence projection of the diffraction vector, is always vertical.

Crystals 100mm diameter and up to 35mm thickness, have been grown on $(\bar{2}\bar{1}\bar{1})$ oriented GaAs seed wafers. Details of the growth system can be found in reference [16]. Samples were cut as rectangular prisms, the longest faces being parallel to $(0\bar{1}1)$ and $(\bar{1}11)$ planes in the un-twinned material (Fig. 3). Faces A and C were 11mm in width, while the B and D faces were each 9mm in width. They were lapped, then polished using a 3 μ m diamond suspension on fabric polishing pads and finally etched for two minutes in a solution of 2% bromine in methanol at 21°C to remove the residual strain associated with the polishing process. As is also evident in Fig. 3, both twinned and un-twinned material will diffract in the $0\bar{2}2$ and $0\bar{4}4$ reflections, whereas the $\bar{1}11$ and $\bar{3}33$ reflections, referenced to the GaAs substrate orientation, will only reveal un-twinned material. In contrast, use of the skew 400 reflection shows only twinned material.

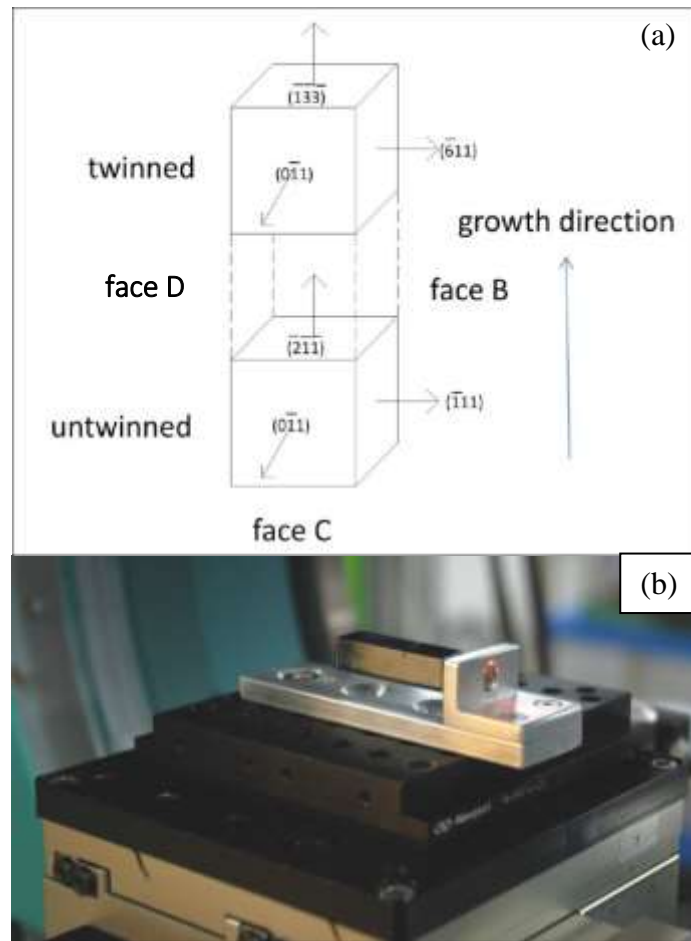


Fig. 3 (a) Schematic diagram of the specimen orientation and imaged faces in both twinned and un-twinned material referenced to the GaAs substrate. (b) Photograph of a sample mounted on the goniometer. The long dimension is in the growth direction and the GaAs seed end is to the right nearest the mounting stub.

4. Results

A considerable amount of information on the crystal lattice perfection can be obtained by reference to Fig. 2 which shows a Renninger “Zebra Pattern” of contours of effective misorientation from superposition of every 8th frame across the rocking curve. The crystal was nucleated on the GaAs substrate as pure CdTe and initially, at the right hand edge of the image, there appears to be strong columnar growth. Zn was injected after several mm of growth. As the image is displaced on the detector, in the vertical direction, due to the change of lattice constant, we can track the Zn composition accurately. Here the Zn gradient is approximately linear with growth length and the enhanced intensity arises from the overlapping of the image during the injection sequence. Following the initial Zn injection, the Zn content drops gradually as crystal growth continues due to maintenance of a constant source temperature and subsequent depletion of the Zn charge for this particular growth recipe.

The Zebra stripes prior to Zn injection are more widely spaced than after injection, revealing that there is greater curvature across the wafer when Zn is incorporated. In particular, there is a diagonal boundary XY, beyond which the curvature is much greater, as evidenced by the closely spaced stripes. There is a continuous variation of

tilt of about 0.4° across the crystal face. No evidence of substantial polygonization was found. The white lines parallel to the growth front to the right of the position marked X are not understood, though they may represent fluctuations in composition. The (light) localised defect regions are attributed to residual polishing damage and there is no evidence, either in the X-ray topographs or in transmission infrared images, of any Te inclusions.

Figure 4 provides an example of how the complete, continuous, image can be reconstructed by adding images with small angular displacement across the full rocking curve. This is the $0\bar{4}4$ reflection from face C of another sample (69-2) cut from the same crystal, and it provides similar information to that of Fig. 2. We note that as the Zn source becomes depleted, the lattice parameter reverts to that of CdTe, as would be expected. The bands parallel to the growth front appear again and there is a noticeable band of contrast at position Z some time after the maximum Zn concentration had been reached. The gap in the image at the far right is a displacement due to tilt, normal to the diffraction vector projection, across a crack which developed close to the seed due to differential contraction between the crystal and GaAs seed on cooldown.



Fig.4. $0\bar{4}4$ reflection composite image of face C of sample 69-2 formed by summing all images taken at 7.2 second steps across the rocking curve. Image width 35 mm and height 8.5 mm.

In the $\bar{3}33$ reflection from face B of sample 69-1, Fig. 5, only un-twinned material is imaged. As in Fig. 4, we note that shortly after the maximum in the Zn concentration, there is a region of lattice distortion (Z) where the growth is much less perfect than prior to Zn injection. Despite the perfection subsequently improving, there appears to be instability in the growth which eventually results in the crystal twinning at F. Two observations are worthy of remark. The first is that un-twinned material is still imaged after the twinning boundary at F. The second is that the boundary, delineated by an absence of intensity in the image due to a lattice twist associated with the twin boundaries, does not appear to run parallel to the growth front. However, one must be cautious, as the differing tilt across the crystal face results in image distortion. This is exemplified by the left hand edge of the image in Fig. 5, where the image is terminated by the straight edge of the incident beam slits, but the diffracted image is curved. It is not possible to determine from our data whether or not the twinning transition takes place simultaneously across the whole growth front. However, what is clear is that the transition takes place across the whole crystal over a relatively short space of time during growth.

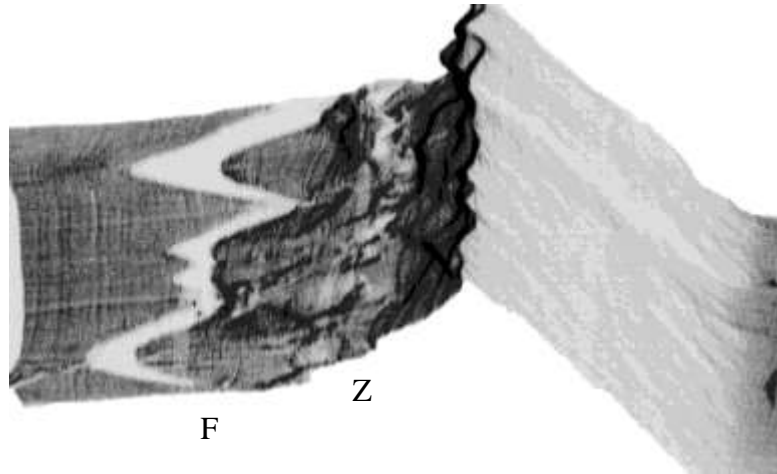


Fig. 5 Composite image of all images taken in 7.2 second steps across the rocking curve for sample 69-1. $\bar{3}33$ reflection from face B. The image is of only un-twinned material. Image displaced at flip boundary F but contrast remains after twinning occurs. Imaged area is 8 mm horizontal by 9 mm vertical.

The presence of an image on the far left of Fig. 5 is evidence for an intermixing of twinned and un-twinned material in that region. Absence of any visible twin boundaries indicates that the scale of the twinning is below the $3.25\mu\text{m}$ resolution of the detector. Use of the charge coupled device (CCD) camera at beamline B16, manufactured by PCO.Imaging GmbH and with optics giving a resolution of $1\mu\text{m}$, also failed to resolve any twin boundaries.

In contrast, the 400 reflection image, (referenced with respect to the twin material orientation), in Fig. 6 only appears after the twinning transition. We note that some twinning takes place in the highly distorted region denoted Z in Fig. 5 but the majority of the twinning takes place at the abrupt boundary F. As the sample is a section cut from the larger boule, it is impossible to say if the initial twinned material grows out into the adjacent material or whether the twinning transition is reversed, but it is evident that there is a delicate energy balance between the two configurations. Fig. 6(a) is a fully integrated image which shows similar characteristic bands parallel to the growth front as presented in Figs. 4 and 5. Fig. 6(b) is a zebra pattern image summed every 8th step and taken with a sample displacement of 10 mm from Fig. 6(a). The contours of effective misorientation are apparent and we note that two distinct regions develop as the crystal grows. On either side the contours are quite widely spaced, indicating modest tilt, whereas between these regions there is a band of closely spaced contours. These contours become closer as the crystal continues to grow, eventually forming a low angle grain boundary.

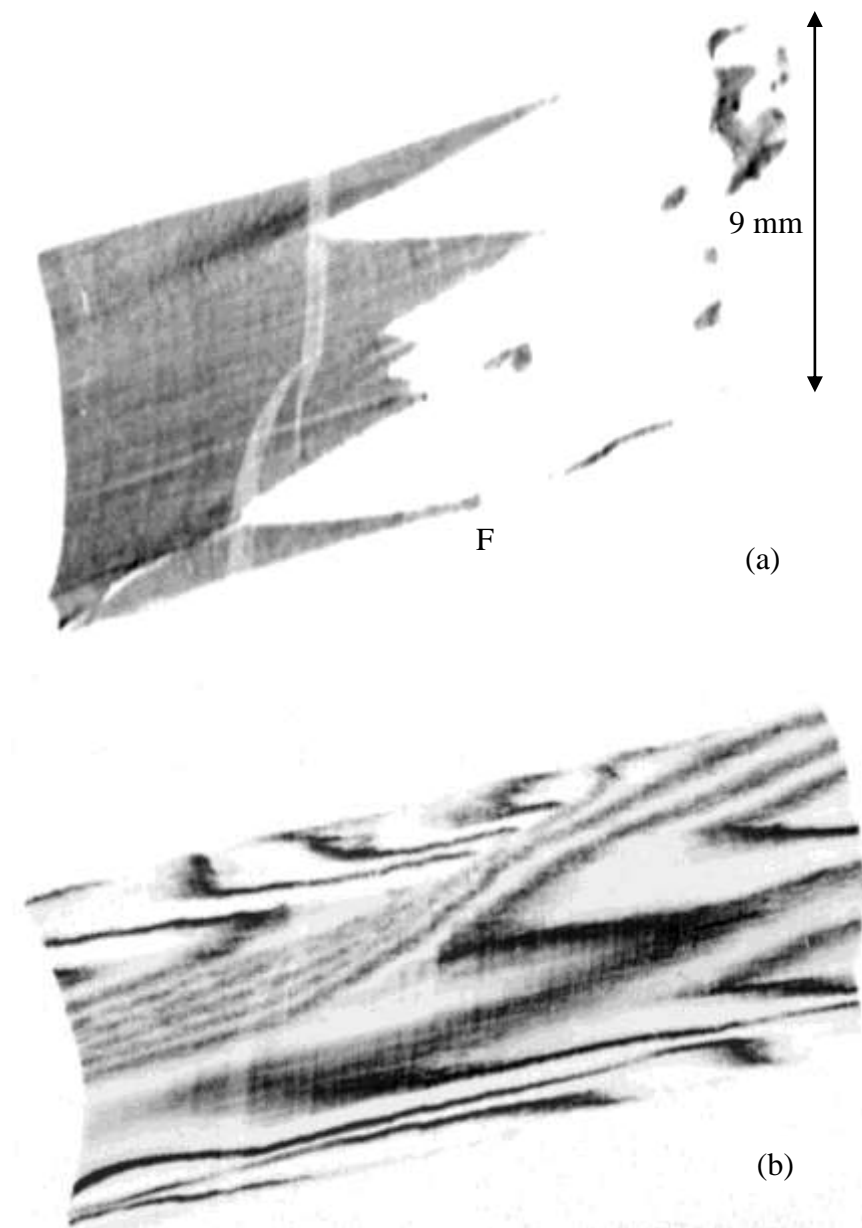


Fig. 6. (a) 400 reflection image from face B of sample 69-1. Step size again 7.2 arc seconds; the composite is formed by adding every image. Image width 6 mm and projected height 9 mm (b) Zebra pattern from summation of images every 8th step from a region of the sample 10 mm to the left of Fig 6(a). [The light pair of almost vertical images, which appear in the same place in (a) and (b) are artefacts on the imaging camera. They can also be found on some other images.]

Not all crystals show such large uniformity in the mixture of twinned and un-twinned material. Fig. 7 shows the $\bar{3}\bar{3}\bar{3}$ reflection from another sample (cut with equivalent faces). Here, the sample is reversed and the image is of face D, opposite to face B. As in the previous example, there is a region of unstable growth, A, after which the growth perfection recovers. There is no disruption to growth on injection of Zn although quite strong growth bands are observed parallel to the growth front, indicating that the temperature control may have been poorer in this growth run. As growth continues the growth bands become more and more distorted until, beyond about 12mm from the seed there is significant contortion. Beyond about 15 mm, the

composite image becomes a zebra pattern as the contours of equal misorientation are no longer uniform and each 7.2 arc second step across the rocking curve results in a significant change of intensity at each point. There appear to be regions where the distortion is substantial, revealed by narrow bands of intensity contour, interspersed with regions that are relatively uniform.

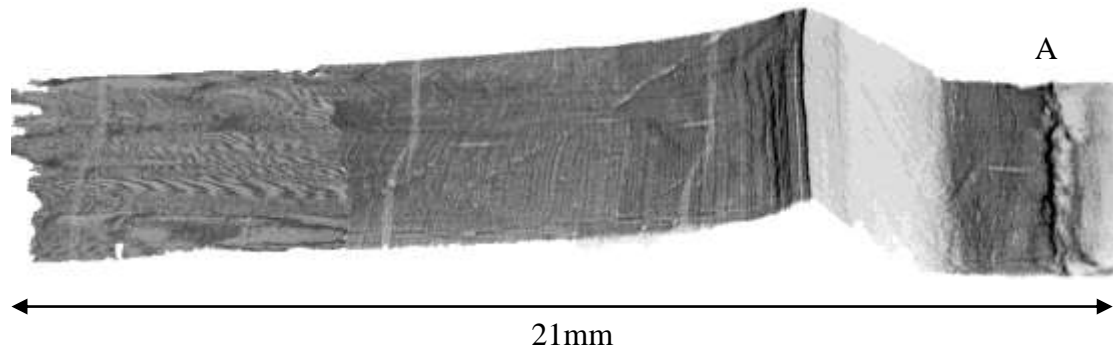


Fig. 7. $\bar{3}\bar{3}\bar{3}$ reflection from a sample cut from a second crystal (number 80-1) which does not reveal an abrupt twinning transition. Note the region of imperfection at A, and the steady disruption of the bands parallel to the growth front beyond about 11mm from the seed (at right hand edge of image). Image 9 mm in height.

Inspection of the composite 400 image from face D, which shows only twinned material (Fig 8), reveals that twinning does not take place until about 14 mm from the seed. The transition is not abrupt and fingers of twinned material interleave with un-twinned crystal. Further, unlike the first crystal, the twinned material does not remain continuously once nucleated, but rather there appears to be a flip back to material of the original orientation.

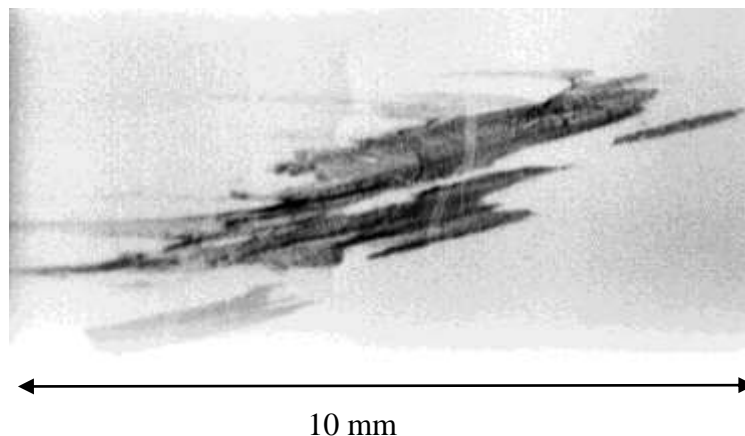


Fig. 8. 400 reflection from face D of the second crystal (80-1). Right hand edge of image is 14 mm from the seed.

While it is not possible to map individual features from Fig 7 to Fig 8 due to the skew nature of the 400 reflection in the twinned material, the finger-like nature of the twinned material is similar to the shape of the misorientation contours at the far left of

Fig. 7. Once again, twinned and un-twinned material must coexist in this region, as contrast is always observed in the $\bar{3}\bar{3}\bar{3}$ reflection (Fig. 7).

5. Discussion

The diffraction imaging experiments have revealed a number of features associated with the $(\bar{2}\bar{1}\bar{1})$ to $(\bar{1}\bar{3}\bar{3})$ twinning transition in bulk $\text{Cd}_{1-x}\text{Zn}_x\text{Te}$ crystals grown on $(\bar{2}\bar{1}\bar{1})$ GaAs substrates. Specific reflections can be found that occur only in un-twinned or twinned material, but not both. Also, because the twinning operation is not coherent across the $(\bar{2}\bar{1}\bar{1})$ planes, there is a 2.53° misorientation between the $(\bar{1}\bar{3}\bar{3})$ twinned and $(\bar{2}\bar{1}\bar{1})$ un-twinned planes. It is therefore straightforward to determine the onset of twinning. This approach also shows that where twinning takes place, un-twinned material also remains adjacent to it and that the scale of the twinning, i.e. distance between twin boundaries, is sub-micron as there are no images of such fine scale structures in the diffraction images. Notwithstanding, in the case where twinning did not occur abruptly, there are well defined boundaries between material in which twinning has taken place and material that retains the original orientation. Under such circumstances, the regions where twinning has occurred must still be a mixture of twinned and un-twinned material. From rocking curve data, we already knew that untwinned material existed after the flip to the twinned orientation, but these measurements provided no information on the scale or nature of the defects. The X-ray diffraction imaging results are consistent with the observation by high resolution electron microscopy that the predominant defect in $\text{Cd}_{1-x}\text{Zn}_x\text{Te}$ thin films are lamellar twins and that they occur at high density [30].

The second observation is that the twinning transition is not related to strain associated with the change in lattice parameter that occurs during the injection of Zn. Despite the Zn composition gradient from the CdTe grown initially being intentionally high, there is no correlation between composition and the onset of twinning, an observation consistent with the occurrence of twinning in pure CdTe itself.

Thirdly, despite both crystals described here having regions of disturbed CdTe buffer growth, in which strain contrast can be observed in the diffraction topographs (Z in Fig. 5 and A in Fig. 7) such strain does not nucleate substantial twinning. In both cases the growth subsequently improved to give un-twinned material of good lattice perfection. Previous studies of the twinning transition have been on thin film material grown by molecular beam epitaxy. Using high resolution transmission electron microscopy Nakamura *et al.* [31] determined the structure of the $(\bar{1}\bar{3}\bar{3})$ CdTe // $(\bar{2}\bar{1}\bar{1})$ GaAs interface and suggested that this arrangement results in greatly reduced lattice mismatch at the interface. Lange *et al.* [32] and Yin *et al.* [33] have also observed dual epitaxy of thin (a few μm) CdTe layers on $(\bar{2}\bar{1}\bar{1})$ oriented GaAs seeds in which the epilayer can be made to grow in either $(\bar{2}\bar{1}\bar{1})$ or $(\bar{1}\bar{3}\bar{3})$ orientation depending on the growth conditions. Lange *et al.* found that the growth orientation obtained depended on the details of the seed preparation, particularly the heat clean, while Yin *et al.* attributed the difference in orientation to difference in growth temperature.

We have already noted that there is a 2.53° misorientation between the $(\bar{2}\bar{1}\bar{1})$ and $(\bar{1}\bar{3}\bar{3})$ in the un-twinned and twinned material respectively and therefore the relationship shown in Fig. 3 is only an approximation. A net 2.53° rotation around the $[0\bar{1}1]$ direction is often observed in heteropitaxy and this occurrence of interfacial tilting contributes in a decrease of the lattice mismatch between substrate and epilayer. Under such conditions, the $(\bar{2}\bar{1}\bar{1})$ surface is entirely converted to $(\bar{1}\bar{3}\bar{3})$.

However, in the present case of growth of CdTe, (and subsequently $\text{Cd}_{1-x}\text{Zn}_x\text{Te}$), on GaAs substrates, the growth begins in $(\bar{2}\bar{1}\bar{1})$ orientation and energy minimization at the seed/crystal interface cannot be the driving force behind the switch from one orientation to the other. This does appear to be in contrast to the MTPVT growth of pure ZnTe on $(\bar{2}\bar{1}\bar{1})$ GaAs, where no evidence of $(\bar{2}\bar{1}\bar{1})$ oriented material could be obtained in the X-ray diffraction images. For ZnTe, the complete transformation to $(\bar{1}\bar{3}\bar{3})$ oriented material occurs very close, if not at, the substrate [13].

It is not obvious from the X-ray diffraction images what drives the twin formation and energetically, the barrier between the two configurations must be low. Twinning on the $\{1\bar{1}1\}$ planes may occur from instability of the growth front, which could come from local strain or temperature instability. There is evidence to support the latter hypothesis from the striation contrast parallel to the growth front seen in the topographs. In this scenario, twinned crystal may propagate laterally, forming a mixture of the two surface planes. These high index planes are not expected to be flat, and due to their higher energy, reverse annihilation of the $\{1\bar{1}1\}$ twinning could occur, as observed experimentally. However, we observe that, in the X-ray diffraction images, twinning invariably starts at a point, suggesting that local strain, associated perhaps with defects or impurities, may nucleate the twinning.

A complicating factor is the appearance of facets on the surface of the growing crystal when the twinning from $(\bar{2}\bar{1}\bar{1})$ to $(\bar{1}\bar{3}\bar{3})$ occurs in the MTPVT material. These facets are also observed to nucleate at a point and develop in a $[\bar{1}11]$ direction as the boule grows. An example, in this case from a pure CdTe crystal is shown in Fig.9. The facets develop as triangles of apex angle 44° and retain this angle as they expand. This angle corresponds to the intersection of two $\{111\}$ planes with the growing surface for both $(\bar{2}\bar{1}\bar{1})$ and $(\bar{1}\bar{3}\bar{3})$ oriented material and these planes are therefore coherent twin boundaries. The interface between twinned and untwinned material at the third side of the facet is more complex and may be responsible for the generation of defects in the material. Facet formation is driven by free energy reduction and it is possible that this term may be the critical factor in providing the driver between the twinned and un-twinned configurations. The facets are associated with opaque defects in infra-red transmission as shown in Fig. 10(a). These defects may be voids or polycrystalline regions as shown in the cross section, Fig. 10(b).

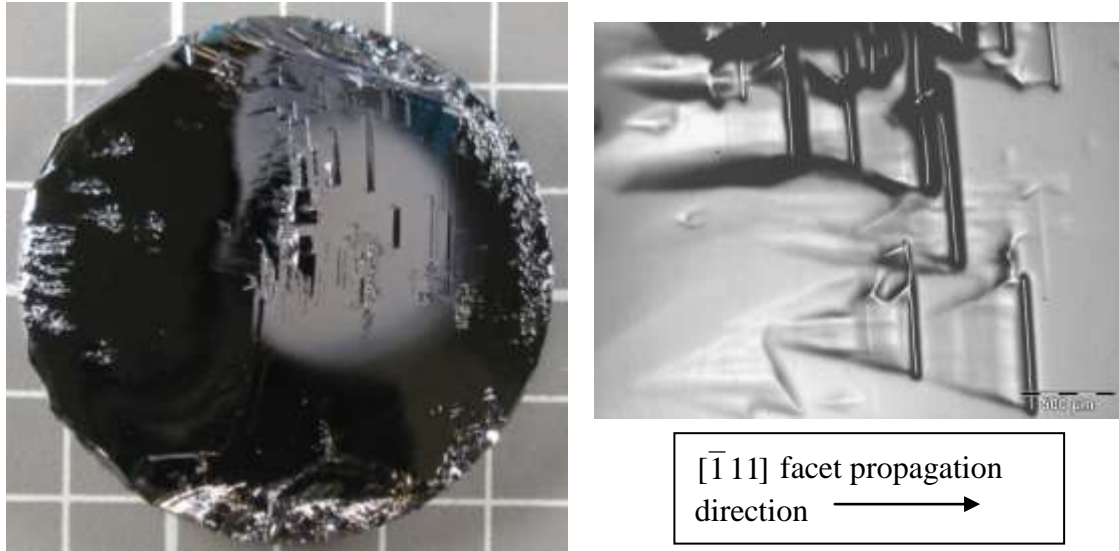


Fig. 9. (a) Photograph of the upper surface of a 8 mm thick CdTe boule grown on a $(\bar{2}\bar{1}\bar{1})$ GaAs seed. Triangular facets have begun to form at the onset of twinning to the $(\bar{1}\bar{3}\bar{3})$ orientation. The boule is 50 mm in diameter. (b) Enlarged portion of the faceted surface showing the 44° apex angle of the triangular facet.

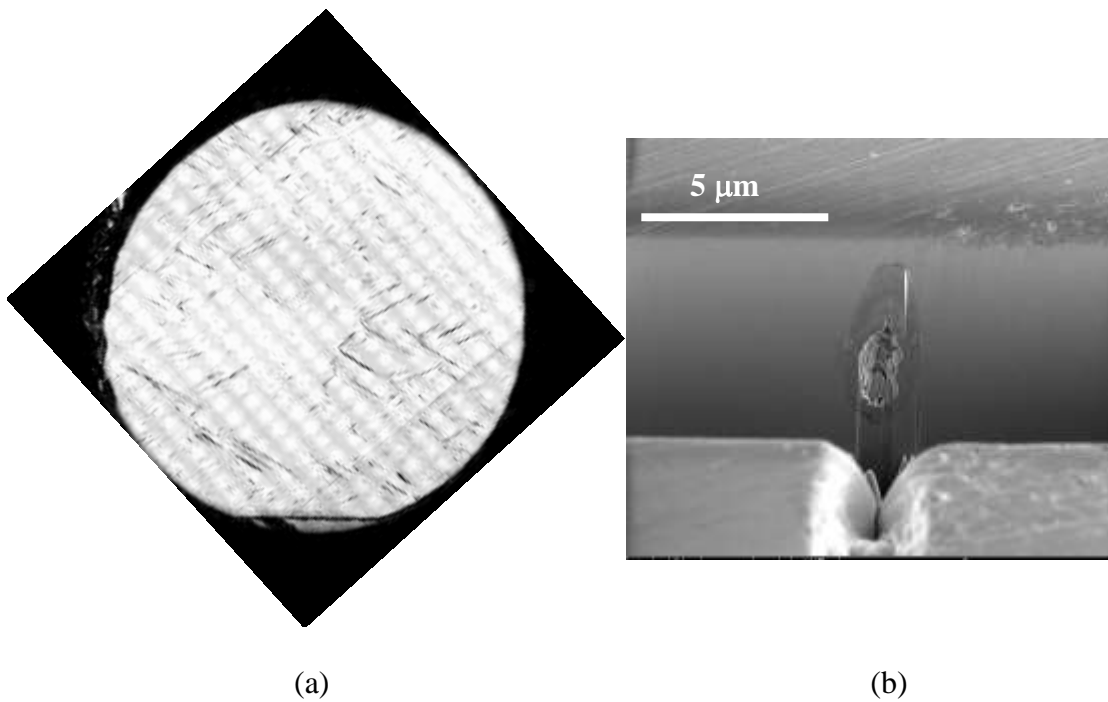


Fig. 10. (a) Infra-red transmission image of a wafer cut in the region of facet formation. The wafer diameter is 50 mm. (b) Secondary electron image of a cross section through an opaque defect fabricated by focussed ion beam milling showing a void and possible polycrystalline material.

6. Conclusions

The driving mechanism for twinning between $(\bar{2}\bar{1}\bar{1})$ and $(\bar{1}\bar{3}\bar{3})$ growth in large volume $\text{Cd}_{1-x}\text{Zn}_x\text{Te}$ crystals growth by physical vapour transport on $(\bar{2}\bar{1}\bar{1})$, also often referred to as (211)B, GaAs substrates remains unclear. Our results indicate the misfit strain relief mechanism proposed to account for the phenomenon in thin film epitaxial growth is not appropriate. As indicated by high resolution X-ray diffraction analysis, a substantial amount of un-twinned material remains once twinning has taken place and the low energy for twinning determined by density functional theory calculations [34] suggests that there is very little difference in the total free energy between either configuration.

Acknowledgements

The authors wish to acknowledge J. Herod for assistance with focussed ion beam milling and electron microscopy. Sincere thanks are expressed to Slava Kachkanov, Kawal Sawhney and the staff of B16 at the Diamond Light Source for excellent technical support.

References

- ¹ A. Zappettini, L. Marchini, M.Z. Zha, G. Benassi, N. Zambelli, D. Calestani, L. Zanotti, E. Gombia, R. Mosca, M. Zanichelli, M. Pavesi, N. Auricchio, E. Caroli, , *IEEE Trans. Nucl. Sci.* **58** (2011) 2353-2356
- ² K.C. Mandal, S.H. Kang, H. Sung, M. Choi, J. Wei, L. Zheng, L. Zhang, G.E. Jellison, M. Groza, A. Burger *J. Electronic Mater.* **36** (2007) 1013-1020
- ³ C-H. Su, S.L. Lehoczky *J. Crystal Growth* **319** (2011) 4-7
- ⁴ G. Q. Li, S-J. Shih, S.C Mu, Y.D. Xu, W.Q Jie *J. Mater. Res.* **25** (2010) 1298-1303
- ⁵ D. M. Hofmann, W. Stadler, P. Christmann, B. K. Meyer, 1996 *Nucl. Inst Meths A* **380** 117-120
- ⁶ G. Li, X. L. Zhang, H. Hua, W. Jie, *J. Electron. Mater.* **34** (2005)1215-1224
- ⁷ U. N. Roy, S. Weiler, J. Stein, *J. Cryst. Growth* **312** (2010) 2840-2845
- ⁸ U. N. Roy, S. Weiler, J. Stein, A. Hossain, G. S. Camarda, A. E. Bolotnikov and R. B. James, *J Crystal Growth* 332 (2011) 34-38
- ⁹ H Chen, S. A. Awadalla, K. Iniewski, P. H. Lu, F. Harris, J. Mackenzie, T. Hasanen, W. Chen, R. Redden, G. Bindley, I. Kuvvetli, C. Budtz-Jørgensen, P. Luke, M. Amman, J. S. Lee, A. E. Bolotnikov, G. S. Camarda, Y. Cui, A. Hossain, R. B. James, *J Appl. Phys.* (2008) **103** 014903
- ¹⁰ U. N. Roy, A. Burger, R. B. James, *J. Cryst. Growth* 379 (2013) 57-62
- ¹¹ A Choubey, P Veeramani, A T G Pym, J T Mullins, P J Sellin, A W Brinkman, I Radley, A Basu, B K Tanner, 2012 *J. Crystal Growth* **352** 120-123
- ¹² A. Schneider, M. C. Veale, S. J. Bell, D. D. Duarte, M. D. Wilson, P. Seller, S. W. Botchway, A. Choubey, D. Halliday, *Phys. Stat. Sol. (a)* (2014) **211** 2121-2125
- ¹³ J. T. Mullins, F. Dierre and B. K. Tanner, *J. Crystal Growth* (2015) **413** 61-66
- ¹⁴ J. T. Mullins, B. J. Cantwell, A. Basu, Q. Jiang, A. Choubey, A. W. Brinkman, B.K. Tanner, *J. Electronic Materials* **37** (2008) 0361-5235
- ¹⁵ J. T. Mullins, B. J. Cantwell, A. Basu, Q. Jiang, A. Choubey, A. W. Brinkman, J. *Crystal Growth* **310** (2008) 2058

-
- ¹⁶ J.T. Mullins, J. Carles, N.M. Aitken, A.W. Brinkman, *J. Crystal Growth* **208** (2000) 211-218.
- ¹⁷ N. M. Aitken, M. D. G. Potter, D. J. Buckley, J. T. Mullins, J. Carles, D. P. Halliday, K. Durose, B. K. Tanner, A. W. Brinkman, *J. Crystal Growth* **198-199** (1999) 984-7
- ¹⁸ D. K. Bowen and B. K. Tanner, 1998 High resolution X-ray diffractometry and topography, (Taylor and Francis, London) pp 252 + x
- ¹⁹ G. A. Carini, G. S. Camarda, Z. Zhong, D. P. Siddons, A. E. Bolotnikov, G. W. Wright, B. Barber, C. Arnone, R. B. James, *J. Electronic Materials* **24** (2005) 804-810
- ²⁰ C. K. Egan, A. Choubey, M. Moore, R. J. Cernik, *J. Crystal Growth* **343** (2012) 1-6
- ²¹ W. Palosz, D. Gillies, K. Grasza, H. Chung, B. Raghothamachar, M. Dudley, *J. Crystal Growth* **182** (1997) 37-44
- ²² M. Renninger *Phys Lett* **1** (1962) 106-9
- ²³ M. Renninger *Z. Angewandte Phys*, **19** (1965) 20-33 and 34-35
- ²⁴ L. Jacobs, M. Hart, *Nucl Inst Meths A*, **173** (1977) 319-25
- ²⁵ M. Hart *J Crystal Growth* **55** (1981) 409-27
- ²⁶ T. Ishikawa, T. Kitano and J. Matsui, *Jap J Appl Phys*, **24** (1985) L968-L971
- ²⁷ S. J. Barnett, G. T. Brown, B.K. Tanner, *Inst Phys Conf Ser*, **87** (1987) 615-620
- ²⁸ See Supplementary Material for video of the contour stripe moving across the crystal as the incidence angle is increased
- ²⁹ S.A. Awadalla, J.Mackenzie, H.Chen, B.Redden, G.Bindley, M.C.Duff, A.Burger, M.Groza, V. Buliga, J.P.Bradley, Z.R.Dai, N.Teslich, D.R.Black, *J. Crystal Growth* **312** (2010) 507–513
- ³⁰ Z.B. He, I. Stoltichnov, N. Setter, M. Cantoni, T. Wojciechowski, G. Karczewski, *J. Alloys and Compounds*, **484** (2009) 757-762
- ³¹ Y.Nakamura, N.Otsuka, M.D.Lange, R.Sporcken, J.P.Faurie, *Appl.Phys.Lett.* **60** (1992)1372–1374.
- ³² M.D. Lange, R.Sporcken, K.K.Mahavadi, J.P.Faurie, Y.Nakamura, N.Otsuka, *Appl. Phys.Lett.* **58** (1991) 1988–1990.
- ³³ J. Yin, Q. Huang, J.M.Zhou, J.G.Yin, *Thin Solid Films* **292** (1997) 303–306.
- ³⁴ W.-J. Yin, J.-H. Yang, K. Zaunbrecher, T. Gessert, T. Barnes, Y. Yan, S.-H. Wei, *Appl. Phys. Lett.* **107** (2015) 141607